Design approach of an axial flux motor for electrical powertrain vehicle

Guillaume Krebs, Eric de Cecco, Claude Marchand

Design approach of an axial flux motor for electrical powertrain vehicle

G. Krebs, E. de Cecco, C. Marchand

***Abstract* – In this paper, an axial flux motor is designed for an electrical powertrain vehicle. The sizing is based on the losses during a driving cycle. A 2D equivalent model is proposed for the axial flux motor. The main features of the optimized motor are given and finally verification is carried out using a 3D finite element calculation code.**

***Index Terms*—permanent magnet synchronous motor, motor design, axial flux motor, reluctance network, finite element method.**

I. INTRODUCTION

For about fifteen years, there are renewed interests in electric vehicles [1]. This is due to several reasons, such as environmental problems (greenhouse gas emissions notably) or the next difficulties for oil supplying. It is a market that may prove promising in all sectors (research, production,...). The main challenges are the cost of the vehicle and his reduced autonomy compared to the traditional combustion engine vehicles.

It is therefore necessary to reduce losses. The total losses can be reduced by sizing adequately the powertrain and particularly the electromechanical conversion [2]. In previous works, a design approach has been proposed for this case [3].

A more detailed design is proposed here on an axial flux motor previously studied. The used methodology constitutes the structure of this paper. The first part is dedicated to the studied motor an axial one with one stator and two rotors. In the second part, the homemade tool software is presented. Some driving cycles are implemented and a barycenter parceling can be used to exploit easily the volume data. Based on constraints (volume, electrical informations,…) the design software include several optimization algorithms for the sizing of the motor and its associated converter. The following part concerns the used model in the homemade software. Results about the most favorable motor are then given and the structure is finally simulated in 3D.

II. STUDIED STRUCTURE

The studied structure is an axial flux motor with inserted permanent magnets and concentrated coils. Previous designs have been already studied in [3]-[5]. This kind of structure offers an interesting power/mass ratio when the axial length is limited. Axial flux motors are well adapted in wheel applications as well as the clutch. Such a structure has been adopted for its simple design.

A brief recall of its structure is done in the following. One quarter of the motor is given in Fig.1. The stator is composed of 6 concentrated coils mounted on tooth and connected in parallel. Stator elements are assumed stuck and maintained by resin.

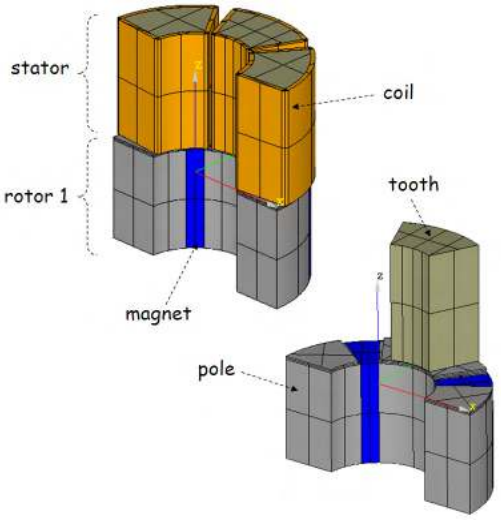

Fig. 1. Geometry of the studied axial flux motor

The two rotors are composed of iron powder alternated with permanents magnets; each one having four magnetic poles. Iron powder is considered having an isotropic permeability.

III. HOMEMADE SOFTWARE AND BARYCENTER MODELING

A homemade software tool is developed under MATLAB™ which aim is to help sizing permanent magnets motors. A sensitivity analysis part allows determining influent factors which should be used for optimization part. It is based on fractional factorial design with Taguchi method [3]. Some analytical and numerical models of motors are now available and some optimization algorithms as genetic, simplex methods and DIRECT [6] are implemented.

A. Driving cycles and barycentric parceling

In conventional approaches, electrical machines are generally designed with a good efficiency for a given operating point. Consequently, the poor performances in variable speed cases mean an increase in volume and therefore in cost of the battery pack.

Torque and speed applied on vehicle with thermal engine during driving cycles are used in this paper. Data are issued from “Artemis cycles” [7], see Fig. 2. Although these data have been extracted from conventional vehicles, such cycles can be adapted for hybrid or full electrical vehicles. The sampling time is constant and equal to 1s.

The authors are with the Laboratoire de Génie Electrique de Paris (LGEP - CNRS UMR 8507 Supelec, Univ. Paris-Sud, UPMC-P6), 11 rue Joliot Curie, 91192 Gif-sur-Yvette, France.
(guillaume.krebs@lgep.supelec.fr).

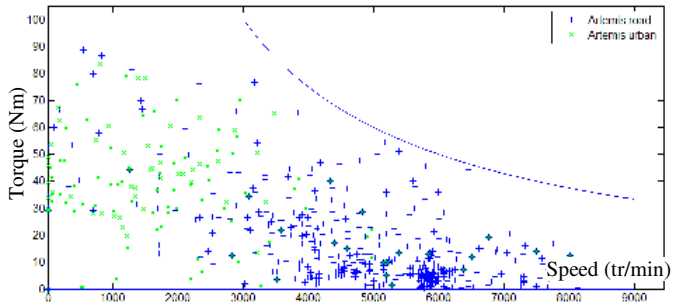

Fig.2. Artemis cycles, road and urban

So, an optimal design would lead to a motor having the minimum of energy lost during driving cycles. Furthermore, the optimal structure must be able to reach extreme torque or speed values. In a first approach, a structure could be found using each operating points of the cycles. If the motor is modeled with long time computing models, this strategy is not attractive.

Consequently, the aim of the proposed approach is to design a powertrain taking into account firstly the two operating points (T_n, Ω_n) and (T_d, Ω_d) (Fig.3) as constraints. The torque-speed space is then separated in some chosen regions (five colored regions in Fig.3). Each area is represented by a center of mass (barycenter) weighted by the number of points inside it. All areas represent the whole space and are included in an objective function.

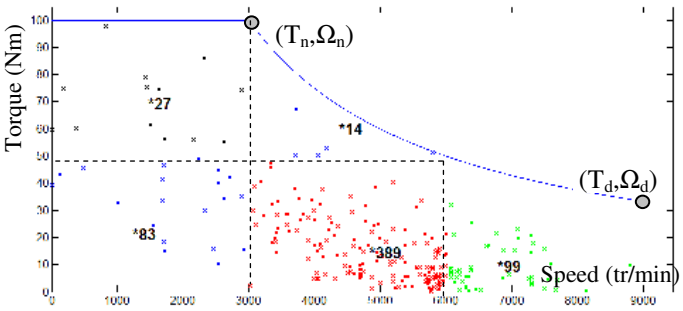

Fig. 3. Artemis cycle, divided in five regions with its number of points

B. *Barycenter modelling*

Energetic criteria mean that the losses have to be calculated. Five parameters are required to calculate the losses on each barycenter located in a region *i*.

$$Bary_i = \begin{cases} \langle \Omega \rangle_i & \text{mean speed} \\ \langle T \rangle_i & \text{mean torque} \\ \langle \Omega^2 \rangle_i^{1/2} & \text{square mean speed} \\ \langle T^2 \rangle_i^{1/2} & \text{square mean torque} \\ N_{pt} & \text{Number of points of the area i} \end{cases} \quad (1)$$

The Joule effect losses ($E_{J\,i}$) for a region *i* having N_{pt} points, are given by (2).

$$E_{J\,i} = \Delta t . \sum_{k=1}^{Npt} R . I_k^2 \quad (2)$$

where *R* is the resistance of the winding and Δt the duration of each point. I_k is linked to the torque by relation (3).

$$T_k = \alpha_k . I_k \quad (3)$$

where α_k is a scalar.

All α_k are assumed equals in a region i. So, its expression is given by (4), for each region i.

$$\alpha_i = \frac{\langle T \rangle_i}{I_i} \quad (4)$$

Where $<T>_i$ is the mean torque of the barycenter of considered area and I_i the value of motor current corresponding to the torque $<T>_i$.

Finally:

$$E_{J\,i} = R . N_{pt} . I_i^2 . \frac{\langle T^2 \rangle_i}{\langle T \rangle_i^2} \quad (5)$$

$<T>$ and $<T^2>$ are calculated when determining the barycenters.

Joule effects (E_J), iron losses (E_{iron}) and converter losses (E_{inv}) can be calculated as shown below.

For every operating point k, iron energetic losses per unit of volume, E_{iron}, is expressed in (6):

$$E_{iron} = \left(k_h . f . \Delta B_k^2 + k_e . \frac{1}{T} \int_0^T \left(\frac{dB}{dt} \right)^2 dt \right) . \Delta t \quad (6)$$

Where k_h and k_f are coefficients calculated from iron manufacturer data, *1/T* is the electrical frequency and *B* the flux density in the considered volume.

Assuming ΔB_k is the same for every point, E_{iron} is given in (7):

$$E_{iron} = . \frac{k_h . p}{2\pi} . N_{pt} . \Delta B^2 . \langle \Omega \rangle + \frac{k_e . p^2}{8} N_{pt} . \Delta B^2 . \langle \Omega^2 \rangle \quad (7)$$

For inverter, E_{inv} takes into account switching (8), recovery (9) and conducting losses (10), for IGBTs and reverse diodes [9].

$$E_{inv\ switching} = N_{pt} . \left(\frac{6}{8} E.tr. I^2 / I_n . f_{sw} + \frac{6}{3\pi} E.tr. I / I_n . f_{sw} + \frac{1}{24} I / I_n \right) \quad (8)$$

$$E_{inv\ recovery} = N_{pt} . 6 . E . f_{sw} . \left[0.28 + \frac{0.38 . I}{\pi . I_n} + 0.015 \left(\frac{I}{I_n} \right)^2 * Q_{rr} + \left(\frac{0.8}{\pi} + 0.05 \left(\frac{I}{I_n} \right) \right) * I * t_{rr} \right] \quad (9)$$

$$E_{inv\ conducting} = N_{pt} . \left[\left(\frac{1}{8} . \frac{0.6}{160} . I_{sw}^2 \right) * 2 + \frac{1}{2\pi} . V_{ce0} . I_{sw} \right] \quad (10)$$

where *E* is the DC bus voltage, f_{sw} the frequency switching, *I* the current motor, I_n the rated current of IGBTs, Q_{rr} the recovery charge, t_{rr} the duration of recovery phenomenon, *tr* the rise time of the current and V_{ce0} the conducting voltage of IGBTs.

C. *Performance*

A previous work [3] shows that the choice of only five barycenters is sufficient to correctly approximate the torque-speed space as shown in Fig. 2. Energetic losses E_j, E_{iron} and E_{inv} computed by the analytical model describes below, are calculated for all points and for the five barycenters (see Table 1). It shows that the relative error is less than 10%.

TABLE 1.
Comparison of total energetic losses calculated (Joules)

	E_j	E_{iron}	E_{inv}
5 Barycenters	69221	725889	566108
All points	63317	713895	602813
Relative error	9.3%	1.7%	6.1%

D. *Objective function and constraints*

As presented previously, the objective (11) and constraint (12) functions are given below.

$$Fobj = \sum_{i=1}^{5} w_i \left| E_{Joule} + E_{iron} + E_{inverter} \right|_{\Omega=\Omega i} \quad (11)$$

$$F_{constr} = \left| T - T_n \right|_{\Omega=\Omega n} + \left| T - T_d \right|_{\Omega=\Omega d} + \left| \Omega - \Omega_n \right|_{\Omega=\Omega n} + \left| \Omega - \Omega_n \right|_{\Omega=\Omega d} = 0 \quad (12)$$

where w_i is the weight associated to a barycenter, Ω_n is the base speed and Ω_d is the high speed.

IV. 2D Equivalent Model

In order to simplify the design of the axial flux motor, a 2D equivalent modelling is proposed [3]. The equivalence is illustrated in Fig.4.

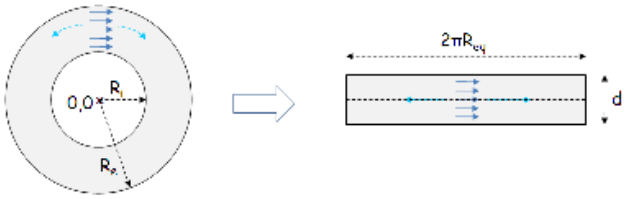

Fig. 4. Axial to 2D equivalent transformation

The picture on the left represents one active surface of the axial flux motor (top view). Arrows in solid line represent coarsely the tangential forces. An equivalent representation (on the right) of the axial active surface is possible using equations (13) and (14). This representation conserves the same active surface and torque value.

$$R_{eq} = \sqrt{\left(\frac{R_e^{\,2} + R_i^{\,2}}{2} \right)} \quad (13)$$

$$d = \frac{R_e^{\,2} - R_i^{\,2}}{2 * R_{eq}} \quad (14)$$

This transformation leads to the 2D linear model given in Fig.5 where half part of the axial flux motor is represented. The parameter *l_p* is the pole width, *la* the magnet width, *l_t* the tooth width, *h_t* the tooth height and *h_p* the pole height.

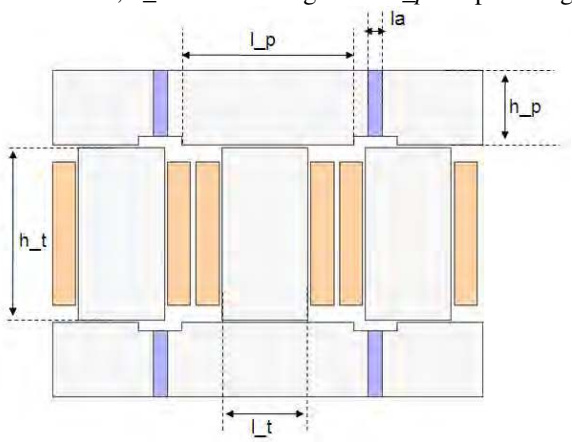

Fig. 5. 2D equivalent model of the studied axial flux motor

V. Reluctance Network Model

A. *Description*

In a design procedure where optimization algorithms are used, reluctance network models present an acceptable compromise between accuracy and computation time. The 2D equivalent model can be discretized as follow.

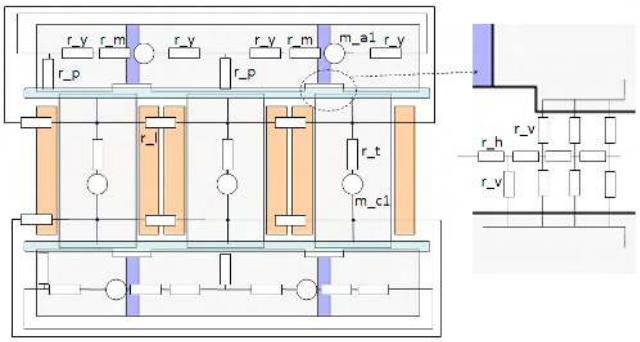

Fig. 6. Reluctance network model

The magnetic materials are supposed to have a linear behaviour and a constant magnetic permeability. The tooth, yoke and magnet reluctances *r_t*, *r_y*, *r_p* and *r_m* are constant and do not depend on the position of the rotors. Flux leakages are taken into account with *r_l*. The sources *m_cx* and *m_ax* represent the magnetomotives forces created by the coils and permanent magnets respectively.

The airgap is discretized by a set of horizontal reluctances *r_h* and vertical reluctances *r_v* whose expressions are given hereafter.

$$r\_h = \frac{dv}{\mu_0 . a . d} \quad (15)$$

$$r\_v = \frac{a/2}{\mu_0 . dv . d} \quad (16)$$

Where *dv* is the step of discretization, *a* is the airgap value, *d* is the depth of the machine and μ_0 the relative permeability. The reluctances *r_v* are only present under the poles and teeth. The slot between two poles is not taken into consideration assuming that the magnetic fluxes flow only through the area where the airgap is minimal.

To solve the problem a matrix system is inverted. The source terms are the magnetomotive forces and the unknowns are defined by the nodal potentials [8]. The model is established under MATLAB™.

After resolution, flux linkages, electromotive forces, instantaneous torque (by mean of virtual works), average torque and losses are computed.

B. *Use of the model*

In this part the procedure used to obtain the operating points in the torque-speed space with the reluctance network model is described.

The inputs of the models are the geometry parameters (see, Fig.5), the current density and the maximum phase to neutral voltage.

The first step is to perform a map (current and phase shift values) of the motor in terms of flux linkages, flux density in ferromagnetic parts, see the diagram on Fig.7 (n_i=20 and n_h=18).

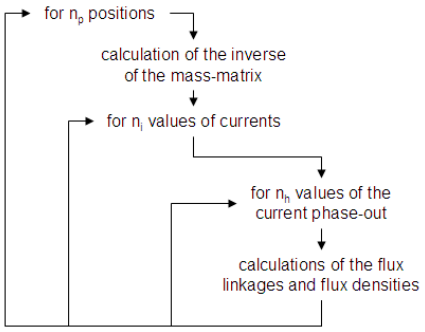

Fig. 7. Procedure used for the map of the motor

In a second step, the derivatives of the flux linkages with respect to the position are calculated in order to obtain the average torque and electromotive forces. For each pair of current value and phase-shift, the maximal values of the derivative are saved. The average torque of the motor is computed with the derivatives of the flux linkages and currents.

The third step consists in determine the line current and phase-shift values required for the operating point. Fig.8 shows the average torque function of maximal current and phase-shift. In this plot, find a contour of isovalues (50Nm for example) is given.

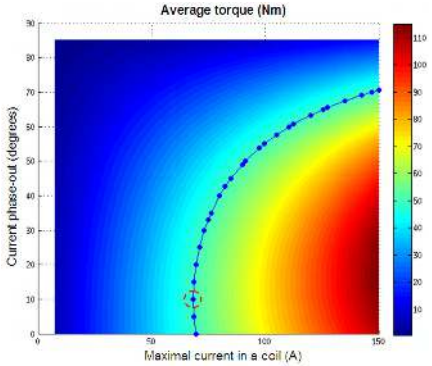

Fig. 8. Procedure used for the map of the motor

The line current and phase-shift values required correspond to the point where the induced voltage is lower than the DC bus (see for example the dot surrounded on Fig.6). When it is possible, the lower value for the line current is chosen

The last step consists to determine the losses. The Joule effects and converter losses can be directly obtained. The line currents and intrinsic parameters (resistance, …) are only needed.

The iron losses per volume are calculated using (6). A map of iron losses is calculated on basis of the results obtained in the first step and for the required motor speed. Such a map is visible on Fig.9.

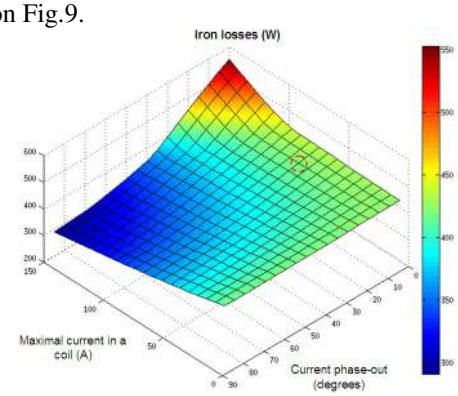

Fig.9. Iron losses map for a given speed

For the line current and phase-shift values required, the iron losses are then interpolated from the map.

VI. Sized and Optimized Powertrain

The previous model has been coupled with the optimization algorithm DIRECT using (11) and (12). The motor sizes satisfying the constraints are summarized in table 2.

TABLE 2.
Optimized motor sizes

R_e	150mm
R_i	51mm
Current density	5.5A/mm²
l_p	140mm
la	6.39mm
h_p	95.7mm
h_t	41.7mm
l_t	92.6mm

The progress of the objective function during the optimization process is presented in Fig.10. First, the objective function value is high, due to penalities, and decreases very quickly. Since the 39th evaluations of the objective function, DIRECT has converged and attempts to reduce the losses.

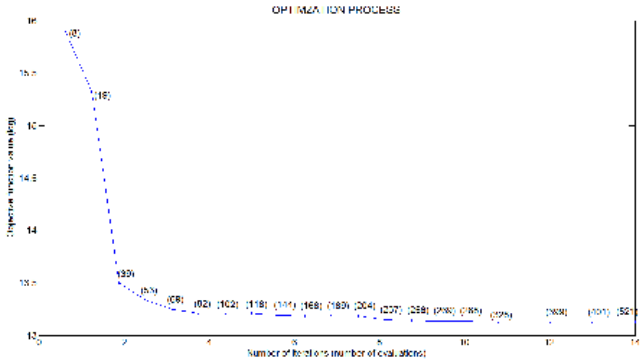

Fig.10. Objective function logarithm values during optimization process

To show the optimized powertrain, different quantities are presented in the torque-speed space.

First of all, Fig.11 and Fig.12 show that the constraints on voltage motor and torque are respected.

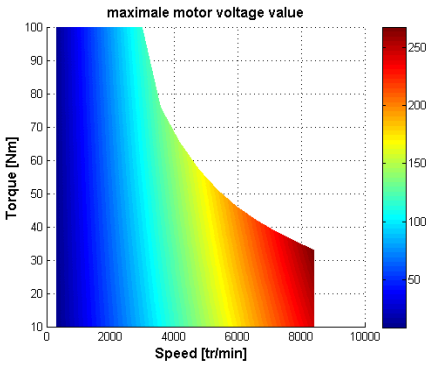

Fig. 11. Maximal motor voltage

The optimization part has reduced total losses, particularly near the region where the vehicle runs the most, see Fig.12.

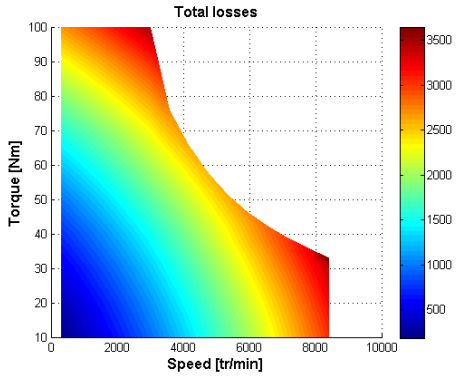

Fig.12. Total losses

The efficiency mapping, Fig.13, shows that the greatest value is not in the region where the vehicle is drived the most. It is the reason why it is necessary to express the objective function in terms of energy and not power.

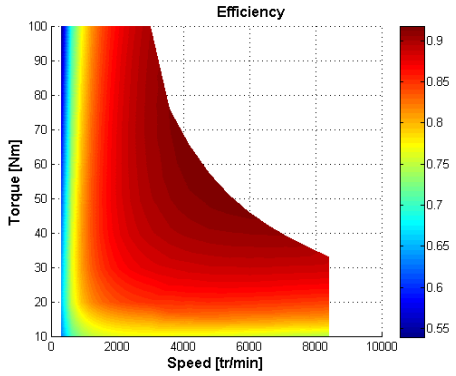

Fig. 13. Efficiency of powertrain

VII. FINITE ELEMENT COMPARISONS

In this part, some comparisons between the reluctance network model and 2D / 3D finite element methods are carried out. The aim of the 2D finite element method is to test the reluctance network model itself. To verify the assumptions proposed in the paragraph 3, the use of 3D finite elements is then proposed.

A. *2D finite element*

Calculations have been performed with the software FEMM [13]. The same geometry as the reluctance network is used. The Fig.14 shows the flux density when the motor is not loaded. The number of elements is about 15000 and the nodes about 8000. In ferromagnetic parts, the B-H relationship is supposed to be linear with a relative permeability equal to 1000. The coercive field of the permanent magnet is 950000 A/m.

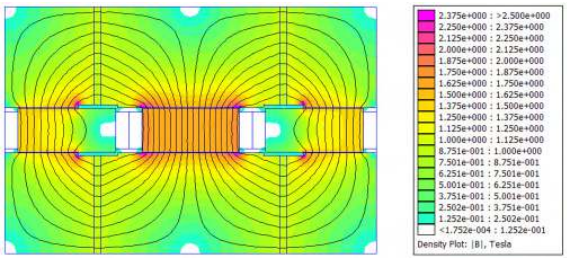

Fig.14. Flux density at no load

B. *3D finite element*

At first the motor (one quarter) with the optimum sizes has been modeled and meshed with *Plateform Salome* [14], see Fig.15. The mesh is composed of 147000 tetrahedra and 30700 nodes.

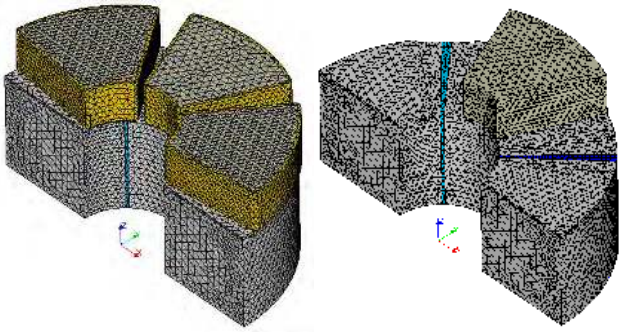

Fig. 15 Mesh of the 3D model

The finite element software is *Code_Carmel 3D* from the laboratory *L2EP* [10] [11]. The used finite element formulation is based on the introduction of a scalar potential Ω and a magnetic source field $\mathbf{H_s}$ such as:

$$\mathbf{H} = \mathbf{H_s} + \mathbf{grad}(\Omega) \qquad (17)$$

The problem is solved by mean of the conjugate gradient method. The movement is taken into account with the *overlapping finite element method* [12]. The torque is calculated with the help of virtual work method.

C. *Comparisons*

The first comparison carried out is about the linkage flux, see Fig.16(a) and (b). The results from the three approaches are closed from each other. This fact is expected due to the linear B-H relationship.

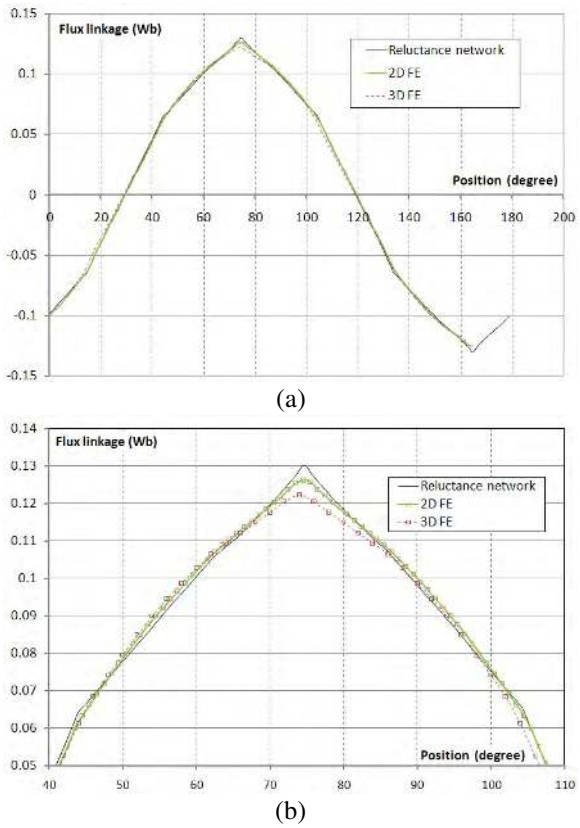

Fig.16. Flux linkage for one coil (a) and zoom (b)

Fig.17 and Fig.18 represent the torques without and with coils powered (150 A max with no phase-shift). The results

issued from the 2D models are in good agreement, although some ripples on 2D FE are probably due to the remeshing at each step of movement.

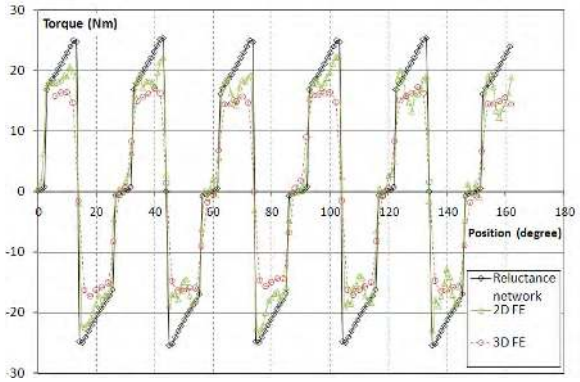

Fig.17. No load torque

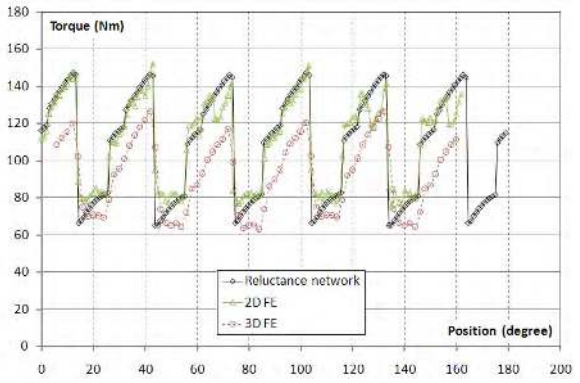

Fig.18. Load torque

However, it can be noticed that there is a significant difference between the 2D and 3D models. In reality the flux density is not uniform following the radius, contrarily to the 2D assumptions. Consequently the repartition of the tangential forces is not uniform leading to an error of the calculation of the torque. This fact is not a problem for the flux linkage because the calculation is performed for all the internal section of the coil.

For this structure, the cogging torque is important, see Fig. 17. Due to the salience, the loaded torque has very important ripples, see Fig.18.

VIII. Conclusion

In this paper, a design approach of an axial permanent magnet motor has been carried out. The sizing has been performed using a minimization of the motor and converter losses during a driving cycle. A 2D model based on a reluctance network has been used. The optimized structure has been compared to a 3D model.

Several aspects have to be studied for future works. The first one will take into account the magnetic saturation. Due to the important load torque ripples, the numbers of magnetic poles and teeth has to be taken into account in optimization procedure. The shift of the two rotors has also to be taken into account.

IX. References

[1] M. Zeraoulia, M.El Hachemi Benbouzid and D. Diallo, "Electric Motor Drive Selection Issues for HEV Propulsion Systems: A Comparative Study", IEEE Trans. on Vehicular Technology, vol. 55, no. 6, pp.1756-1764, november 2006.

[2] J. Lindstrom, J. Hellsing, and J. Luomi, "Design of high-efficiency electrical motors for a hybrid electric vehicle",*13th International Electric Vehicle Symposium*, EVS-13, Osaka, 1996.

[3] E. de Cecco, G. Krebs, C. Marchand, "Design of electric powertrains for vehicles using driving cycles", *Conference Compumag*, Sydney, Australia, July 2010.

[4] Patent EP1276213, "Machine discoide", inventors: J. Saint Michel, A. Abou-Akar, Applicant: Leroy-Somer, publication date: 2003-01-15.

[5] O. Maloberti, C. Marchand, Y. Choua, D. Condamin, L. Kobilansky, E. Bomme, "Multi-Physical quasistatic modelling of an axial flux permanent magnet machine", *International Conference on Electrical Machines (ICEM)*, Roma, Italy, Sept. 2010.

[6] http://www4.ncsu.edu/~ctk/Finkel_Direct/

[7] "Impact of the gearshift strategy on emission measurements", Artemis 3142 report, Report n° LTE 0307 March 2003.

[8] G. Krebs, A. Tounzi, B. Pauwels and D. Willemot, "Modelling and control of a 2D of PM synchronous actuator using Hall effect sensors", *Mechatronics*, vol. 20, n°. 1, pp. 153-161, February 2010.

[9] F. Casanellas, "Losses in PWM inverters using IGBTs", *IEE Proceedings on Electric Power Applications*, vol. 141, n°. 5, pp. 235-239, Sept. 1994.

[10] Y. Le Menach, S. Clenet, F. Piriou, "Determination and utilization of the source field in 3D magnetostatic problems", IEEE Transactions on Magnetics, Vol. 34, N°. 5, pp. 2509-2512, Sept. 1998.

[11] T. Henneron, S. Clénet, J. Cros, P. Viarouge, "Evaluation of 3-D Finite Element Method to Study and Design a Soft Magnetic Composite Machine", IEEE Transactions on Magnetics, vol. 40,N°2, pp 786 – 789, 2004.

[12] H. Zaidi, L. Santandrea, G. Krebs, Y. Le Bihan, E. Demaldent, " Use of Overlapping Finite Elements for Connecting Arbitrary Surfaces With Dual Formulations", IEEE Transactions on Magnetics, Vol. 48, N°. 2, pp. 583-586, Feb. 2012.

[13] http://www.femm.info

[14] http:// www.salome-platform.org